Metabolites of *Latilactobacillus curvatus* BYB3 and indole activate aryl hydrocarbon receptor to attenuate lipopolysaccharide-induced intestinal barrier dysfunction

Authors:
Xing Wang, Cheng Chung Yong, Sejong Oh*

Affiliation:
Division of Animal Science, Chonnam National University, Gwangju 61186, Republic of Korea

Xing Wang (https://orcid.org/0000-0002-0775-9306); wangxing920801@126.com

Cheng Chung Yong (https://orcid.org/0000-0003-0531-6381); yongchengchun@gmail.com

Sejong Oh (https://orcid.org/0000-0002-5870-3038); soh@jnu.ac.kr

Running title: Metabolites of *Latilactobacillus curvatus* BYB3

* Corresponding author:

Sejong Oh

Division of Animal Science, Chonnam National University, Gwangju 61186, Republic of Korea

Contact: +82-62-530-2116

Fax: +82-62-530-2129

E-mail: soh@jnu.ac.kr

Metabolites of *Latilactobacillus curvatus* BYB3 and indole-activate aryl hydrocarbon receptor to attenuate lipopolysaccharide-induced intestinal barrier dysfunction

Abstract

This study aimed to investigate the effects of the metabolites of *Latilactobacillus curvatus* BYB3 and indole-activated aryl hydrocarbon receptor (AhR) to increase the tight junction (TJ) proteins in an *in vitro* model of intestinal inflammation. Western blot analysis showed that the supernatants of *L. curvatus* BYB3, indole, and the metabolites of indole derivatives reduced lipopolysaccharide (LPS) simulated in Caco-2 cells; this was a result of upregulating the expression of TJ-associated proteins, namely zona occludens-1 (ZO-1) and claudin-1 (CLDN-1), and by suppressing nuclear factor-kappa B (NF-κB) signaling. Immunofluorescence images consistently revealed that LPS disrupted and reduced the expression of TJ proteins, while the metabolites of *L. curvatus* BYB3 and indole reversed these alterations. The protective effects of *L. curvatus* BYB3 were observed on the intestinal barrier function when measuring transepithelial electrical resistance. Using HPLC analysis the metabolites, the indole-3-latic acid and indole-3-acetamide concentrations were found to be 1.73±0.27mg/L and 0.51±0.39mg/L, respectively. These findings indicate that the metabolites of *L. curvatus* BYB3 have increasing mRNA expressions of cytochrome P450 1A1 (*CYP1A1*) and AhR, and may thus be applicable for therapy of various inflammatory gut diseases as postbiotics.

Key words:

Latilactobacillus curvatus BYB3; aryl hydrocarbon receptor; Caco-2 cells; tight junctions; lipopolysaccharide

Introduction

Intestinal epithelial cells (IECs) with intact tight junctions (TJs) form a barrier between the external environment and the mammalian host (Yu et al., 2018). Normal functioning of the intestinal epithelial barrier is critical for maintaining health (Citi, 2018; Odenwald and Turner, 2017; Turner, 2009). Disruption of TJs and paracellular permeability can promote the entry of molecules and activate the immune system, leading to continuous tissue destruction (Lee, 2015). Hence, maintaining the integrity of the intestinal epithelial barrier is critical for inhibiting the development of gastrointestinal diseases and inflammation (Tlaskalová-Hogenová et al., 2004).

Indole, an interspecies and interkingdom signaling molecule, plays essential roles in bacterial pathogenesis and eukaryotic immunity (Lee et al., 2015). The human intestinal tract is rich in a diverse range of about 10^{14} commensal bacteria, some of which are crucial for nutrient assimilation and benefit the immune system (Tlaskalová-Hogenová et al., 2004). A metabolomic study demonstrated that the production of indoxyl sulfate and the antioxidant indole-3-propionic acid in animal blood depended entirely on enteric bacteria (Wikoff et al., 2009). In addition, indole and its derivatives may influence human diseases, such as bacterial infections, intestinal inflammation, neurological diseases, diabetes, and cancers (Lee et al., 2015).

Multiple protein complexes, which are crucial components of TJs, are located in IECs (Tsukita et al., 2001) and include occludin, claudins, and zonula occludens (ZO). These protein complexes are vital for the maintenance of TJs and permit cytoskeletal regulation of the intestinal barrier integrity (Van Itallie and Anderson, 2006). Pathogens damage the intestinal epithelial barrier, increase intestinal permeability, and induce the development of inflammatory bowel disease (IBD) and necrotizing enterocolitis (NEC) (Guo et al., 2015). IBD includes two

chronic idiopathic inflammatory diseases, ulcerative colitis, and Crohn's disease. It affects individuals of different ages, including children and the geriatric population, and all aspects of life (Arrieta et al., 2009). Lipopolysaccharide (LPS) is a harmful antigen that can trigger inflammatory responses in the intestinal tissue and can be detected in the serum of patients with NEC and IBD (Han et al., 2020). Recent studies have identified the association between clinically relevant concentrations (1 – 10 ng/mL) of LPS and intestinal barrier dysfunction under in vivo and in vitro conditions (Guo et al., 2013). In our previous study, *Latilactobacillus curvatus* BYB3 decreased the disease activity score of dextran sulfate sodium-induced colitis in a mouse model (Wang et al., 2022). Supplementation with indole or using *Lactobacillus reuteri* with high AhR ligand production can improve some metabolic symptoms (Swimm et al., 2018). Therefore, we hypothesized that *L. curvatus* BYB3 has a similar function. The supernatants of *L. curvatus* BYB3 and the metabolites of *L. curvatus* BYB3+indole ameliorated LPS-induced intestinal barrier dysfunction by upregulating the levels of TJ proteins in Caco-2 cells. These findings illustrated the mechanism underlying the destructive effect of clinically relevant concentrations of LPS on the intestinal epithelial barrier, providing evidence for the clinical application of metabolites of *L. curvatus* BYB3+indole in the treatment of LPS-induced intestinal barrier dysfunction.

The aryl hydrocarbon receptor (AhR) is a ligand-dependent transcription factor that is widely expressed in vertebrates and is involved in numerous biological processes, such as cell proliferation (Xie et al., 2012), apoptosis (Marlowe et al., 2008), differentiation (Xie et al., 2012), and inflammatory response (Neavin et al., 2018). The AhR separates from its molecular chaperone complex and forms a heterodimer with the aryl hydrocarbon nuclear translocator (ARNT) in the nucleus. This AhR-ARNT dimer then binds to the upstream regulatory region of its target genes, such as the cytochrome P450 family 1 genes (*CYP1A1* and *CYP1B1*) (Esser

and Rannug, 2015). Indoles may have utility as an intervention to limit the decline of barrier integrity and the resulting systemic inflammation that occurs with aging (Powell et al., 2020). Indoles and indole-metabolites secreted by the commensal bacteria have been shown to extend the healthspan of diverse organisms, including *Caenorhabditis elegans*, *Drosophila melanogaster*, and mice. The effects of indole and metabolites on animal heatlthspan were found to be AhR-mediated (Sonowal et al., 2017).

This study was conducted to research the effect of *L. curvatus* BYB3 on the intestinal epithelial barrier of the Caco-2 cells. Furthermore, we investigated the differences in mRNA expression levels of CYP1A1 and AhR in response to the metabolites of *L. curvatus* BYB3 and indole.

Materials and Methods

1. Materials

LPS derived from *Escherichia coli* O111:B4 was purchased from Sigma-Aldrich Corp. (Burlington, MA, USA) and dissolved in phosphate-buffered saline (PBS) to prepare the stock solutions with concentrations of 1 mg/mL. DL-indole-3-lactic acid (ILA), 3-indoleacetic acid (IAA), indole-3-acetamide (IAM), and indole were purchased from Sigma-Aldrich Corp., and trifluoroacetic acid was procured from Daejung Chemicals and Metals Co. Ltd. (Gyeonggi-do, Korea). All reagents were stored as specified by the manufacturer. The following antibodies were used in the study: zona occludens 1 (ZO-1) antibody (Cat No.21772-1-AP; Proteintech. Inc., Illinois, USA), claudin-1 antibody (Cat No. ab211737; Abcam, Cambridge, UK), nuclear factor-kappa B (NF-κB) antibody (sc-372; Santa Cruz Biotechnology, Inc., Dallas, TX, USA), p-NF-κB p65 (Cell Signaling Technology, Inc., Danvers, MA, USA), β-actin C4 antibody (sc-

4778; Santa Cruz Biotechnology, Inc., Dallas, TX, USA), secondary R-antibody (Cat. No. A11036; Invitrogen Corp., Waltham, MA, USA), and Westar Supernova (Code.XLS3,0100, Cyanagen, SRL, Bologna, Italy)

2. Indole test

Twenty-one probiotic candidates (Table 2) were cultivated in MRS medium ((Difco™ Lactobacilli MRS broth, BD Diagnostics, Franklin Lakes, NJ, USA) for 24 h at 37℃. Before use, the overnight LABs were diluted to a cell density of 10^7 CFU/mL in MRS broth prior to use. Indole was added at a final concentration of 58.5 mg/mL, and the cells were incubated at 37℃ for 24 h. Then samples were centrifuged at 3500 rpm for 15 min at room temperature. A total of 1 mL of the supernatant was collected and mixed immediately with 0.4 mL of Kovac's reagent to determine the extracellular indole concentration. After the Kovac's reagent was added, the mixture was vortexed to separate the phases. The top phase was collected, and the absorbance was measured at 540 nm.

3. Bacterial cultivation and cell-free supernatant (CFS) harvesting

L. curvatus BYB3 cells were isolated from traditional homemade kimchi in Gwangju and Jeollanam-do, and maintained in MRS broth. Cells were incubated in the MRS broth at 37℃ and centrifuged at 1500×g for 15 min at room temperature to obtain cell pellets. The pellets were stored in 10% glycerol or skim milk at − 80ºC until further use. The supernatant was filtered using a 0.2 µm syringe (Sartorius AG, Gottingen, Germany). The cells in the indole group were treated with 58.5 mg/mL indole, those in the BYB3 group were incubated with *L. curvatus* BYB3, and those in the BYB3+indole group were treated with both *L. curvatus* BYB3 and 58.5 mg/mL indole. The three groups were incubated in the MRS medium for 24 h at 37℃. The cell pellets were discarded, and the CFSs were used to treat the Caco-2 cells.

4. Cell culturing and treatment protocol

The Caco-2 cells used in the study were obtained from the Korean Cell Line Bank (No.30037.1, Seoul, Korea). Caco-2 cells were cultured in Modified Eagles Medium (MEM), high glucose (HyClone, Laboratories, Inc. Logan, UT, USA), supplemented with 20% fetal bovine serum (Gibco™, Thermo Fisher Scientific Inc., Waltham, MA, USA), 1% MEM non-essential amino acids solution (100×) (Gibco™, Thermo Fisher Scientific Inc.), and 1% antibiotic-antimycotic solution (Gibco™, Thermo Fisher Scientific Inc.) at 37℃ in an atmosphere containing 5% CO_2. The medium was replaced every two or three days. The Caco-2 cells (1×10^6 cells) were seeded in a 20 × 90 mm dish and treated with 10 ng/ mL of LPS. They were then treated with 1 mL of indole, 1 mL of *L. curvatus* BYB3, and 1 mL of the BYB3+ indole metabolites supernatants.

5. Transepithelial electrical resistance (TEER) assay

Caco-2 cells (1×10^3 cells/cm^2) were seeded in a Corning®, Costar®, Transwell® chamber with 0.4 μm pores (Corning Inc, New York, NY, USA) that had been placed in a 24-well plate. Another Transwell® plate was kept blank. After reaching confluence, the cells were differentiated and polarized for 7–10 days in the culture medium. Subsequently, the Caco-2 cells were treated with 10 ng/mL of LPS and later with 100 μL of indole supernatant, 100 μL of *L. curvatus* BYB3 supernatant, and 100 μL of BYB3+ indole supernatants. The TEER assay was used to measure cell monolayer integrity before and after all treatments. The TEER was measured using an epithelial volt-ohm-meter equipped with a chopstick electrode (Millicell® ERS-2 (Electrical Resistance System), EMD Millipore Corp. Burlington, MA, USA). The electrode was immersed at a 90° angle, with one tip in the basolateral chamber and the other in the apical chamber. Care was taken to prevent contact of the electrode with the monolayer. Measurements were performed in triplicate for each monolayer. An insert without Caco-2 cells

was used as a blank; the mean resistance of the blank was subtracted from all samples. The unit area resistance was calculated by dividing the resistance values by the effective membrane area (0.33 cm^2).

6. RNA isolation and gene expression analysis

Caco-2 cells (1×10^6cells) seeded in a 20×90 mm dish were treated with 10 ng/mL of LPS followed by treatment with 1 mL of indole supernatant, 1 mL of strain 3,15 and LGG supernatant, and 1 mL of indole + strain 3,15 and LGG supernatants. After incubation for 24 h, the cells were collected for further analysis. Total RNA was isolated and converted into complementary DNA (cDNA) as described previously. Briefly, 2 µg of total RNA was used to cDNA using a Maxime RT PreMix kit (Oligo Dt primer) (Cat. No. 25081, iNtRON Biotechnology Inc., Seongnam-si, Gyeonggi-do, Korea). The following primers were used for real-time polymerase chain reaction (RT-PCR) (Table 1)

PCR was performed under the following conditions: initial denaturation at 94℃ for 3 min, followed by 40 cycles of the program with incubations at 94℃ for 30 s, 60℃ for 30 s, and 72℃ for 1 min, followed by incubation at 65℃ for 5 s, until the end of the program. The relative gene expression levels were determined by comparative analyses using the formula:

$$\text{Relative expression} = 2^{-(\Delta Ct)}, \text{ with } C_t = C_{t\ gene} - C_{t\ GAPDH}$$

7. Protein extraction and Western blot analysis

Caco-2 cells (1×10^6 cells) were seeded in a 20 × 90 mm dish and treated with 10 ng/mL of LPS and then 1 mL of the indole supernatant, 1 mL of BYB3 supernatant, and 1 mL of indole+BYB3 metabolites supernatant. After incubation for 24 h, the cells were collected for further analysis.

The total protein concentration in the cell lysates was determined using the PRO-PREP protein extraction solution (iNtRON Biotechnology Inc., Seongnam, Korea). Briefly, 5×10^6 cells were immersed in 400 µL of the PRO-PREP solution and homogenized in ice for 10–20 min. The mixture was then centrifuged at 13000×g at 4℃ for 5 min, and the extracted protein was collected in the supernatant. The protein concentration was determined by the Pierce BCA Protein Assay Kit (Thermo Fisher Scientific Inc.). Equal amounts of protein (50 µg per lane) were separated using 10% sodium dodecyl sulfate-polyacrylamide gel, electroblotted (Mini-PROTEAN® II Cell Systems; Bio-Rad Laboratories Inc., Hercules, CA, USA), and transferred to a polyvinylidene difluoride membrane (Bio-Rad Laboratories Inc.). The proteins were blocked with 5% skim milk (Difco, Detroit, MI, USA) and underwent overnight antibody incubation against E-cadherin, N-cadherin, Vimentin, and β-actin at 4℃. After incubation, the membranes were washed and incubated with horseradish peroxidase-conjugated goat anti-mouse or anti-rabbit antibodies for 1 h at room temperature. After each was washed three times with PBST for 10 min, protein bands developed. The bands were detected via enhanced chemiluminescence, and the band density was determined using β-actin as the reference protein.

8. Immunofluorescence staining of ZO-1, claudin-1, and NF-κB

Caco-2 cells were seeded on a 24-well plate at a density of 1×10^3 cells/mL. These cells were treated with 10 ng/mL of LPS and then with 100 µL each of indole, *L. curvatus* BYB3, BYB3+indole metabolite supernatants. After treatment for 24 h, the cells were collected for the next step.

The cells were prepared as described in Material and Methods. Caco-2 cells were grown on glass coverslips; the slides were washed with PBS for 5 min at room temperature, fixed with 3.7% formaldehyde in PBS buffer for 20 min at 4℃, and again rinsed thrice with PBS buffer for 5 min at room temperature. The monolayers were permeabilized with 0.5% Triton™ X-100

(Sigma-Aldrich Corp.) for 20 min at room temperature and rinsed three times with PBS buffer for 2 min at room temperature. The slides were blocked with 5% skim milk in tris buffered saline with Tween® (TBST) for 1 h at room temperature without rinsing. They were then incubated with rabbit polyclonal anti-ZO-1 antibody, rabbit monoclonal anti-claudin-1 antibody, and rabbit polyclonal anti-NF-κB p65 antibody for 2 h at room temperature. The slides were rinsed thrice with TBST for 5 min at room temperature. The remaining incubations were performed in the dark. The slides were further incubated with an Alexa Fluor® 568 goat anti-rabbit secondary antibody (Abcam, Cambridge, UK). Nuclei were stained using 4‘,6-diamidino-2-phenylindole dihydrochloride (DAPI) (Cat. No D1306; Invitrogen Corp.) for 15 s at room temperature. The samples were covered with a coverslip using the Vectashield® anti-fade mounting medium (Vector cat. #H-1000; Vector Laboratories, Inc., Newark, CA, USA). The edges of the coverslips were sealed by nail polishing. The slides were examined and analyzed using a fluorescence microscope (Olympus BX50, Tokyo, Japan).

9. Analysis of the metabolites in the CFSs by high-performance liquid chromatography (HPLC)

The indole derivatives in the CFSs were analyzed as previously described. Briefly, filtered samples were injected (10 mL), in triplicate, into an HPLC system (Knauer, Wissenschaftliche Geräte GmbH, Berlin, Germany) equipped with a C-18 gravity 150 × 4.6 mm column, particle size: 5 μm (Macherey-Nagel GmbH & Co. KG; Düren, Germany). The flow rate was set to 1 mL/min, and the column oven temperature was maintained at 30℃. The running buffers were 0.3% trifluoroacetic acid solutions prepared in ultra-pure water (A) and acetonitrile (B). The process was initiated with an A:B ratio of 90:10; the linear gradient was applied to reach this ratio in 1 min. The steps included gradients with 55% solution A: 45% solution B for 28 min, 5% solution A: 95% solution B for 30 and 35 min, and 90% solution A: 10% solution B for 36

min. The measurements were stopped after 45 min. The detection wavelength was set at 280 nm.

10. Statistical analysis

All data are presented as mean ± standard deviation (SD) of triplicate experiments. Statistical significance comparing different sets of groups was determined using the Student's *t*-test. In experiments comparing multiple experimental groups, statistical differences between groups were analyzed using one-way analysis of variance (ANOVA). Statistical analyses were performed using IBM® SPSS® Statistics 20 (IBM, Inc., Chicago, IL, USA), and a $p < 0.05$ was considered statistically significant.

Results

1. Indole test result of the probiotic candidates' CFSs

The probiotic candidates (Table 2 and Fig. 1) show the *Lactobacillus* strains' ability to metabolize and reduce indole concentration during fermentation. Among the tested *Lactobacillus* strains, 3 *(L. curvatus* BYB3), 15 (*Lactobacillus. acidophilus*), and 21 (*Lactilacobacillus. rhamnosus GG*) demonstrated remarkable indole reducing abilities and were selected for subsequent analyses.

2. Metabolites of *L. curvatus* BYB3 and indole significantly increased AhR activation in LPS-treated Caco-2 cells

Caco-2 cells were treated with the 10% MRS as the control and 10% supernatant of the strains (3,15 and 21) previously screened for 24 h. Treatment of the Caco-2 cells with 10 ng/ mL of LPS simulated the conditions of colitis. A previous study detected increased expression

of *CYP1A1*, which is indicative of the AhR activation (Yu et al., 2018). To confirm the activation of the AhR by the metabolites, the mRNA expression levels of *CYP1A1* and *AhR* were determined after treating the Caco-2 cells for 24 h with LPS alone or in combination with other supernatants. The supernatants of *L. curvatus* BYB3 and indole significantly increased the mRNA expression CYP1A1 and AhR by 35-fold and 3-fold, respectively (Fig. 2A and 2B).

3. Metabolites of *L. curvatus* BYB3 and indole increased the TEER in LPS-induced Caco-2 cells

The TEER was used to measure cell monolayer integrity, which was assessed before and after all treatments. LPS increased the permeability of the intestinal epithelial barrier. However, the effects of the metabolites of *L. curvatus* BYB3 and indole on the LPS-mediated increase in intestinal permeability are unknown. LPS significantly decreased the TEER after 12 h; the reduction continued for 24 h after application (Fig. 3). In contrast, the metabolites of *L. curvatus* BYB3 and indole remarkably increased the TEER. This finding suggests that the metabolites reduced the permeability of the intestinal epithelial barrier. In addition, the supernatants of *L. curvatus* BYB3 and indole increased the TEER. However, co-treatment with the metabolites and LPS significantly restored the LPS-mediated increase in the permeability of the intestinal epithelial barrier in Caco-2 cells (Fig. 2 and 3). Hence, these metabolites could significantly protect against LPS-induced intestinal permeability.

4. Effect of metabolites of *L. curvatus* BYB3 and indole on the expression of TJ proteins and inflammatory responses in Caco-2 cells

LPS down-regulated the expression of the ZO-1, occludin, and claudin-1 proteins. Caco-2 cells were co-treated with 10 ng/ mL of LPS, the supernatants of indole and *L. curvatus* BYB3, and the metabolites of BYB3+indole for 24 h to determine alterations in the expression

of the TJ proteins. The Caco-2 cells treated with *L. curvatus* BYB3+indole showed increased expression of the ZO-1 and claudin-1 proteins compared to cells treated with LPS alone (Fig 4A and 4B). Furthermore, cells treated with the metabolites of BYB3+indole showed a significant increase in the expression of ZO-1 and claudin-1.

To explore the anti-inflammatory effects of the metabolites on Caco-2 cells, alterations in NF-κB, a biomarker of inflammation, were examined. NF-κB p65 and the protein levels of total and phospho-p65 were detected by Western blot analysis. Compared to the LPS-treated cells (10 ng/ mL, control), the Caco-2 cells treated with the supernatants of *L. curvatus* BYB3, indole, and metabolites of BYB3+indole showed decreased NF-κB expression. The reduction was significant in the presence of the metabolites of *L. curvatus* BYB3+indole. Interestingly, co-treatment with the metabolites of *L. curvatus* BYB3+indole and LPS had a remarkable effect on the attenuation of LPS-induced inflammation.

5. Immunofluorescence of the metabolites of *L. curvatus* BYB3 and indole

Immunofluorescence was used to detect the localization and expression of TJ proteins, as these results were more intuitive. The LPS-treated group showed severe disruption in the structure of TJ proteins structure (Fig. 5). In contrast, the TJ protein ZO-1 was intact without any damage in the cells treated with LPS+BYB3+indole. LPS-induced disruption was repaired in the LPS+indole, and LPS+BYB3 treated groups. Examination of claudin-1 expression revealed a trend similar to that observed for ZO-1 (Fig. 5A and 5B).

Consistent with this observation, immunofluorescence analysis of NF-κB demonstrated that p65 accumulated within the nucleus of Caco-2 cell monolayers treated with the metabolites of *L. curvatus* BYB3+indole. However, incubation with LPS decreased LPS-induced nuclear accumulation of NF-κB (Fig. 5C).

6. Identification and verification of indole compounds in the samples using HPLC

HPLC analysis was performed to precisely identify and quantify indole derivatives. Several indole derivatives (100 μM each) were separated, and their peaks were detected by HPLC using a C-18 reverse column (Fig. 6). Under optimal conditions, the retention times of IAM, ILA, IAA, and indole were 13.2, 16.1, 19.3, and 29.1 min, respectively (Fig. 6A). The peak in Fig. 6B corresponds to the main components because of the presence of indole from the supernatants of the indole-treated 0 h. The three peaks in Fig. 6C represent IAM, ILA, and indole. The main component in Fig. 6C, indicated by three peaks, including two of IAM and one of ILA, represented the supernatant of the *L. curvatus* BYB3 group fermented for 24 h. The indole content in the supernatants of the *L. curvatus* BYB3+indole group was reduced, and IAM and ILA metabolites were observed to varying degrees (Fig. 6D).

Discussion

Indole alleviates the symptoms of gastrointestinal disorders by activating the AhR (Hubbard et al., 2015). Several compounds have been proposed as putative endogenous AhR ligands, many of which are produced via pathways involved in the metabolism of tryptophan and indole, including indole-3-aldehyde (IAld), IAA, and many more (Chung and Gadupudi, 2011) (Bittinger et al., 2003). In our previous study, AhR activation inhibited NF-κB expression, in vivo and in vitro (Salisbury and Sulentic, 2015). In macrophages, the activation of AhR signaling blocks NF-κB binding sites and masks NF-κB transcription activity, suppressing NLRP3 inflammasome activation (Huai et al., 2014). Hence, the current study aimed to identify the potential effect of metabolites of *L. curvatus* BYB3 and indole in mediating the recovery of TJ after LPS-induced disruption of the intestinal barrier in the colon mucosal cell layer. Our preliminary studies showed that *L. curvatus* BYB3 might play a role in

329 alleviating inflammatory responses. However, the association between intestinal TJ proteins
330 and inflammation influenced by *L. curvatus* BYB3 was not elucidated under in vitro conditions.
331 The findings from this study suggest that the metabolites of *L. curvatus* BYB3 and indole can
332 activate the AhR.

333 In previous studies, LPS-induced inflammation disrupted the integrity of IECs and
334 increased paracellular permeability (Gao et al., 2018). The results from this study demonstrated
335 that the supernatants of *L. curvatus* BYB3, indole, and metabolites of BYB3+indole inhibited
336 LPS-induced inflammation in IECs by enhancing the expression of TJ proteins and decreasing
337 paracellular permeability in Caco-2 cells. However, direct evidence is required to explore the
338 association between the supernatants of cells treated with *L. curvatus* BYB3, indole, and the
339 metabolites of *L. curvatus* BYB3+indole and intestinal permeability; such evidence was not
340 available earlier. ZO-1, occludin, and claudin-1 are important TJ proteins that maintain
341 permeability in the small intestine (Anderson and Van Itallie, 1995). Western blot analysis
342 revealed that the administration of the metabolites of *L. curvatus* BYB3+indole significantly
343 improved intestinal epithelial barrier function by increasing the expression of the TJ proteins
344 ZO-1 and claudin-1. Deregulated NF-κB activation has been previously reported to contribute
345 to the pathogenesis of various inflammatory diseases (Liu et al., 2017). In this study, the
346 metabolites of BYB3+indole decreased NF-κB expression.

347 In a previous study, we determined that *Lactobacillus* improved the intestinal epithelial
348 barrier function by increasing the expression of TJ proteins (Zeng et al., 2020). TEER is a
349 commonly used indicator of intestinal epithelial membrane permeability (Srinivasan et al.,
350 2015). An increase in the TEER and a decrease in paracellular permeability reflect the
351 enhancement of the barrier function (Capaldo et al., 2017). The small intestine is one of the
352 main organs of the digestive system, and the Caco-2 cell monolayer is a recognized intestinal
353 cell line.

According to this study's HPLC analysis, only three indole compounds were detected among the metabolites of *L. curvatus* BYB3+indole, namely IAM, indole, and ILA. Several *Bacteroides* spp. and *Clostridium bartlettii* have been reported to produce ILA and IAA, whereas *Bifidobacterium* spp. have been reported to produce ILA (Aragozzini et al., 1979; Russell et al., 2013). However, there are few reports of *L. curvatus* producing ILA.

Our results provide evidence that microbiota-mediated metabolism inhibits LPS-induced inflammation, increasing the expression of TJ proteins. Based on the primary research results of this study, key metabolic molecules that improve intestinal should be investigated in further studies. We demonstrated that the metabolites of *L. curvatus* BYB3 and indole inhibited LPS-induced inflammation in IECs by enhancing TJs, which, in turn, reduced paracellular permeability. HPLC results confirmed that various concentrations of indole and indole derivatives (ILA and IAM) enhance TJ protein expression. This protective effect may provide a potential approach to restoring TJ barrier function, and AhR may be a novel therapeutic target in gut health and diseases such as IBD.

References

Anderson J, Van Itallie C. 1995. Tight junctions and the molecular basis for regulation of paracellular permeability. *Am. J. Physiol. Gastrointest. Liver Physiol* 269:G467-G475.

Aragozzini F, Ferrari A, Pacini N, Gualandris R. 1979. Indole-3-lactic acid as a tryptophan metabolite produced by bifidobacterium spp. *Appl. Environ. Microbiol.* 38:544-546.

Arrieta M-C, Madsen K, Doyle J, Meddings J. 2009. Reducing small intestinal permeability attenuates colitis in the il10 gene-deficient mouse. *Gut* 58:41-48.

Bittinger MA, Nguyen LP, Bradfield CA. 2003. Aspartate aminotransferase generates proagonists of the aryl hydrocarbon receptor. *Mol. Pharmacol.* 64:550-556.

Capaldo CT, Powell DN, Kalman D. 2017. Layered defense: How mucus and tight junctions seal the intestinal barrier. *J. Mol. Med.* 95:927-934.

Chung KT, Gadupudi GS. 2011. Possible roles of excess tryptophan metabolites in cancer. *Environ. Mol. Mutagen.* 52:81-104.

Citi S. 2018. Intestinal barriers protect against disease. *Science* 359:1097-1098.

Esser C, Rannug A. 2015. The aryl hydrocarbon receptor in barrier organ physiology, immunology, and toxicology. *Pharmacol. Rev.* 67:259-279.

Gao Y, Li S, Wang J, Luo C, Zhao S, Zheng N. 2018. Modulation of intestinal epithelial permeability in differentiated caco-2 cells exposed to aflatoxin m1 and ochratoxin a individually or collectively. *Toxins* 10:13.

Guo S, Al-Sadi R, Said HM, Ma TY. 2013. Lipopolysaccharide causes an increase in intestinal tight junction permeability in vitro and in vivo by inducing enterocyte membrane expression and localization of tlr-4 and cd14. *Am. J. Pathol.* 182:375-387.

Guo S, Nighot M, Al-Sadi R, Alhmoud T, Nighot P, Ma TY. 2015. Lipopolysaccharide regulation of intestinal tight junction permeability is mediated by tlr4 signal transduction pathway activation of fak and myd88. *J. Immunol.* 195:4999-5010.

Han Y, Zhao Q, Tang C, Li Y, Zhang K, Li F, Zhang J. 2020. Butyrate mitigates weanling piglets from lipopolysaccharide-induced colitis by regulating microbiota and energy metabolism of the gut–liver axis. *Front. Microbiol.* 11:2930.

Huai W, Zhao R, Song H, Zhao J, Zhang L, Zhang L, Gao C, Han L, Zhao W. 2014. Aryl hydrocarbon receptor negatively regulates nlrp3 inflammasome activity by inhibiting nlrp3 transcription. *Nat. Commun.* 5:1-9.

Hubbard TD, Murray IA, Perdew GH. 2015. Indole and tryptophan metabolism: Endogenous and dietary routes to ah receptor activation. *Drug Metab. Dispos.* 43:1522-1535.

Lee J-H, Wood TK, Lee J. 2015. Roles of indole as an interspecies and interkingdom signaling molecule. Trends in microbiology 23:707-718.

Lee SH. 2015. Intestinal permeability regulation by tight junction: Implication on inflammatory bowel diseases. *Intest Res.* 13:11.

Liu T, Zhang L, Joo D, Sun S-C. 2017. Nf-κb signaling in inflammation. *Signal Transduct Target Ther.*2:1-9.

Marlowe JL, Fan Y, Chang X, Peng L, Knudsen ES, Xia Y, Puga A. 2008. The aryl hydrocarbon receptor binds to e2f1 and inhibits e2f1-induced apoptosis. *Mol. Biol. Cell.* 19:3263-3271.

Neavin DR, Liu D, Ray B, Weinshilboum RM. 2018. The role of the aryl hydrocarbon receptor (ahr) in immune and inflammatory diseases. *Int. J. Mol. Sci.*19:3851.

Odenwald MA, Turner JR. 2017. The intestinal epithelial barrier: A therapeutic target? *Nat Rev Gastroenterol Hepatol.* 14:9-21.

Powell DN, Swimm A, Sonowal R, Bretin A, Gewirtz AT, Jones RM, Kalman D. 2020. Indoles from the commensal microbiota act via the ahr and il-10 to tune the cellular composition of the colonic epithelium during aging. *Proc. Natl. Acad. Sci. U.S.A.* 117:21519-21526.

Russell WR, Duncan SH, Scobbie L, Duncan G, Cantlay L, Calder AG, Anderson SE, Flint HJ. 2013. Major phenylpropanoid‐derived metabolites in the human gut can arise from microbial fermentation of protein. *Mol Nutr Food Res.* 57:523-535.

Salisbury RL, Sulentic CEW. 2015. The ahr and nf-κb/rel proteins mediate the inhibitory effect of 2,3,7,8-tetrachlorodibenzo-p-dioxin on the 3′ immunoglobulin heavy chain regulatory region. *Toxicol. Sci.* 148:443-459.

Sonowal R, Swimm A, Sahoo A, Luo L, Matsunaga Y, Wu Z, Bhingarde JA, Ejzak EA, Ranawade A, Qadota H. 2017. Indoles from commensal bacteria extend healthspan. *Proc. Natl. Acad. Sci. U.S.A.* 114:E7506-E7515.

Srinivasan B, Kolli AR, Esch MB, Abaci HE, Shuler ML, Hickman JJ. 2015. Teer measurement techniques for in vitro barrier model systems. *J Lab Autom*. 20:107-126.

Swimm A, Giver CR, Defilipp Z, Rangaraju S, Sharma A, Ulezko Antonova A, Sonowal R, Capaldo C, Powell D, Qayed M. 2018. Indoles derived from intestinal microbiota act via type i interferon signaling to limit graft-versus-host disease. Blood, *Am. J. Hematol.* 132:2506-2519.

Tlaskalová-Hogenová H, Štěpánková R, Hudcovic T, Tučková L, Cukrowska B, Lodinová-Žádnıková R, Kozáková H, Rossmann P, Bártová J, Sokol D. 2004. Commensal bacteria (normal microflora), mucosal immunity and chronic inflammatory and autoimmune diseases. *Immunol. Lett.* 93:97-108.

Tsukita S, Furuse M, Itoh M. 2001. Multifunctional strands in tight junctions. *Nat. Rev. Mol. Cell Biol.*2:285-293.

Turner JR. 2009. Intestinal mucosal barrier function in health and disease. *Nat. Rev. Immunol.* 9:799-809.

Van Itallie CM, Anderson JM. 2006. Claudins and epithelial paracellular transport. *Annu. Rev. Physiol.* 68:403-429.

Wang X, Li D, Meng Z, Kim K, Oh S. 2022. Latilactobacillus curvatus byb3 isolated from kimchi alleviates dextran sulfate sodium (dss)-induced colitis in mice by inhibiting il-6 and tnf-r1 production. *J. Microbiol. Biotechnol.* 32:348-354.

Wikoff WR, Anfora AT, Liu J, Schultz PG, Lesley SA, Peters EC, Siuzdak G. 2009. Metabolomics analysis reveals large effects of gut microflora on mammalian blood metabolites. *Proc. Natl. Acad. Sci. U.S.A.* 106:3698-3703.

Xie G, Peng Z, Raufman J-P. 2012. Src-mediated aryl hydrocarbon and epidermal growth factor receptor cross talk stimulates colon cancer cell proliferation. *Am. J. Physiol. Gastrointest. Liver Physiol.* 302:G1006-G1015.

Yu M, Wang Q, Ma Y, Li L, Yu K, Zhang Z, Chen G, Li X, Xiao W, Xu P. 2018. Aryl hydrocarbon receptor activation modulates intestinal epithelial barrier function by maintaining tight junction integrity. *Int. J. Biol. Sci.* 14:69.

Zeng Y, Zhang H, Tsao R, Mine Y. 2020. Lactobacillus pentosus s-pt84 prevents low-grade chronic inflammation-associated metabolic disorders in a lipopolysaccharide and high-fat diet c57/bl6j mouse model. *J. Agric. Food Chem.* 68:4374-4386.

Table and Figure Legends

Table. 1. Primer sequences for quantitative polymerase chain reaction (PCR)

Gene	Primer sequences	References
CYP1A1	F: TCGGCCACGGAGTTTCTTC	(Yang et al. 2022)
CYP1A1	R: GGTCAGCATGTGCCCAATCA	
AhR	F: CAAATCCTTCCAAGCGGCATA	(Behfarjam et al. 2018)
AhR	R: CGCTGACCTAAGAACTGAAAG	
GAPDH	F: GAAATCCCA CACCATCTTCC	
GAPDH	R: AAATGAGCCCCAGCCTTCT	

471 **Table. 2. Probiotic candidates tested**

No.	Strains	Abbreviation	Source	Renamed genus (Zheng et al. 2020)
1	*L. curvatus* BYB1	BYB1	Kimchi	*Latilactobacillus curvatus*
2	*L. curvatus* BYB2	BYB2	Kimchi	*Latilactobacillus curvatus*
3	*L. curvatus* BYB3	BYB3	Kimchi	*Latilactobacillus curvatus*
4	*L. curvatus* BYB4	BYB4	Kimchi	*Latilactobacillus curvatus*
5	*L. curvatus* BYB7	BYB7	Kimchi	*Latilactobacillus curvatus*
6	*L. brevis* OB1	OB1	Kimchi	*Levilactobacillus brevis*
7	*L. brevis* OB4	OB4	Kimchi	*Levilactobacillus brevis*
8	*L. brevis* OB3	OB3	Kimchi	*Levilactobacillus brevis*
9	*L. sakei* OB8	OB8	Kimchi	*Latilactobacillus sakei*
10	*L. casei* MYA5	MYA5	Kimchi	*Lacticaseibacillus casei*
11	*L. sakei* JNU533	JNU533	Kimchi	*Latilactobacillus sakei*
12	*L. sakei* MYA6	MYA6	Kimchi	*Latilactobacillus sakei*
13	*L. fermentum* NS4	NS4	Kimchi	*Limosilactobacillus fermentum*
14	*L. amylovorus* CH6	KCNU	Swine intestine	*Unchanged*
15	*L. acidophilus* GP1B	GP1B	Swine intestine	*Unchanged*
16	*L. plantarum* L67	L67	Infant feces	*Lactiplantibacillus plantarum*
17	*L. plantarum* OY1	OY1	Kimchi	*Lactiplantibacillus plantarum*
18	*L. plantarum* OY2	OY2	Kimchi	*Lactiplantibacillus plantarum*
19	*L. fermentum* JNU532	JNU532	Kimchi	*Limosilactobacillus fermentum*
20	*L. fermentum* JNU534	JNU534	Kimchi	*Limosilactobacillus fermentum*
21	*L. rhamnosus* GG	LGG	Human intestine	*Latilactobacillus rhamnosus*

472

473

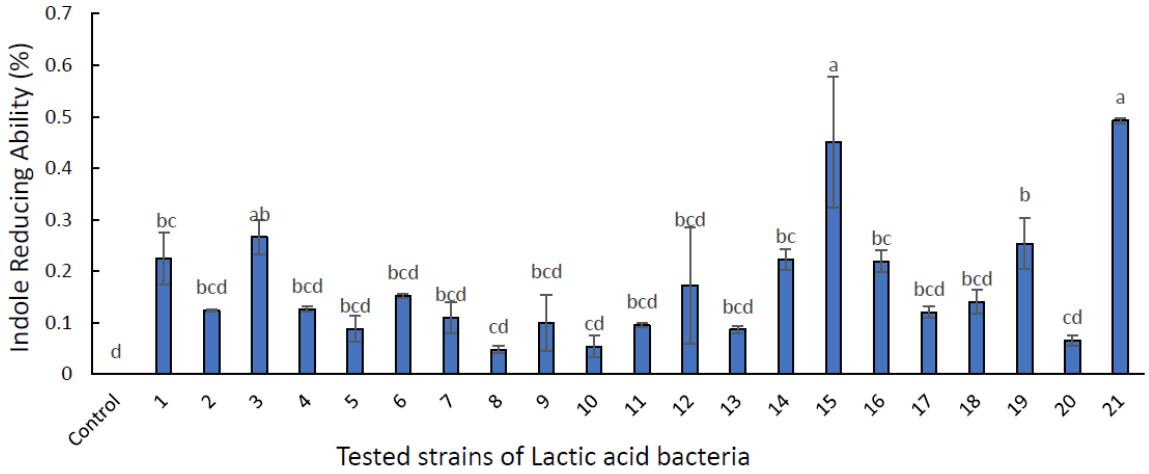

474

475 **Fig. 1. Indole test results of the probiotic candidates' CFSs**

476 Indole test of 21 candidate strains for examination of metabolism. The mean values of the
477 samples are significantly different (indicated by different letters). Different letters indicate
478 significant differences according to the change in indole concentration from low to high. The
479 values of the experimental groups were normalized to those of the control groups, and
480 statistically significant differences are indicated by * $p<0.05$, ** $p<0.01$. Data are presented as
481 the mean ± SD (n = 3).

482

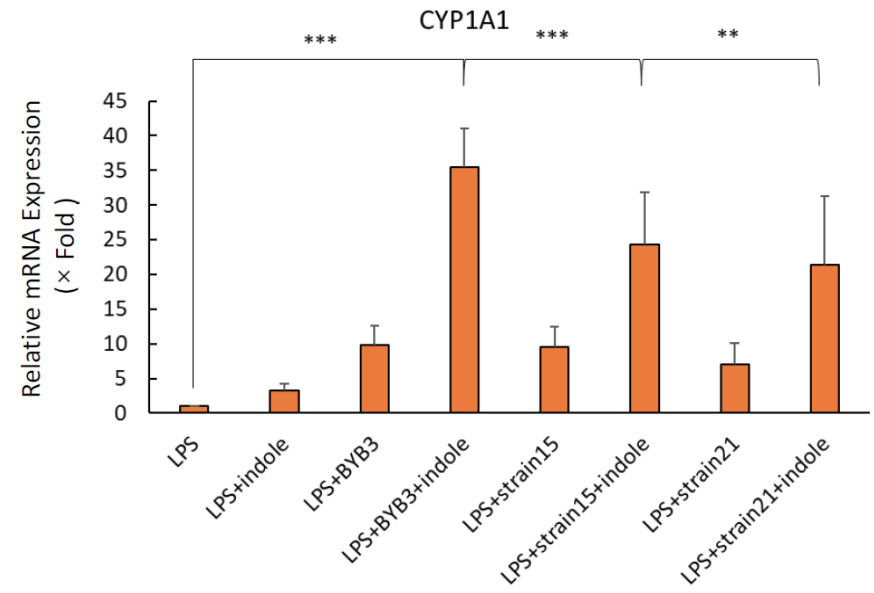

483

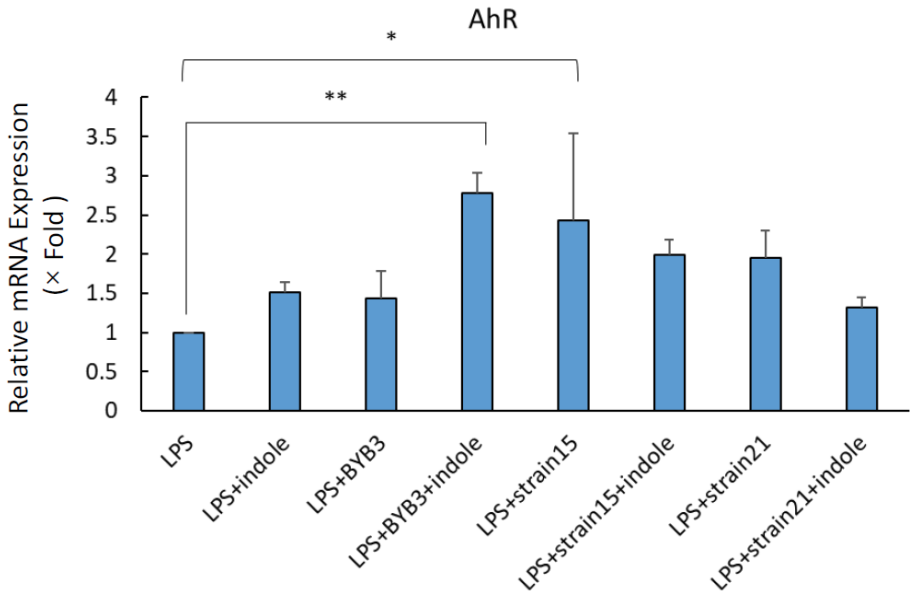

484

485 **Fig. 2. Metabolites of *L. curvatus* BYB3 and indole significantly increased AhR**

486 **activation in LPS-treated Caco-2 cells**

487 (A and B) show the mRNA levels of *CYP1A1* and *AhR* in 10 ng/ mL LPS-induced cells,
488 respectively. The sample sequence is the control (supernatant of the medium MRS), and
489 supernatants after treatment with indole, *L. curvatus* BYB3, BYB3+indole, strain15, strain

490 15+indole, strain21, strain 21+indole, which were added in turn. Different letters indicate the
491 mean values of the samples that are significantly different according to the changes in mRNA
492 expression. Experimental groups were normalized to control groups; statistically significant
493 differences are shown by *p< 0.05 and **p< 0.01. Data are presented as mean ± SD (n = 3).

494

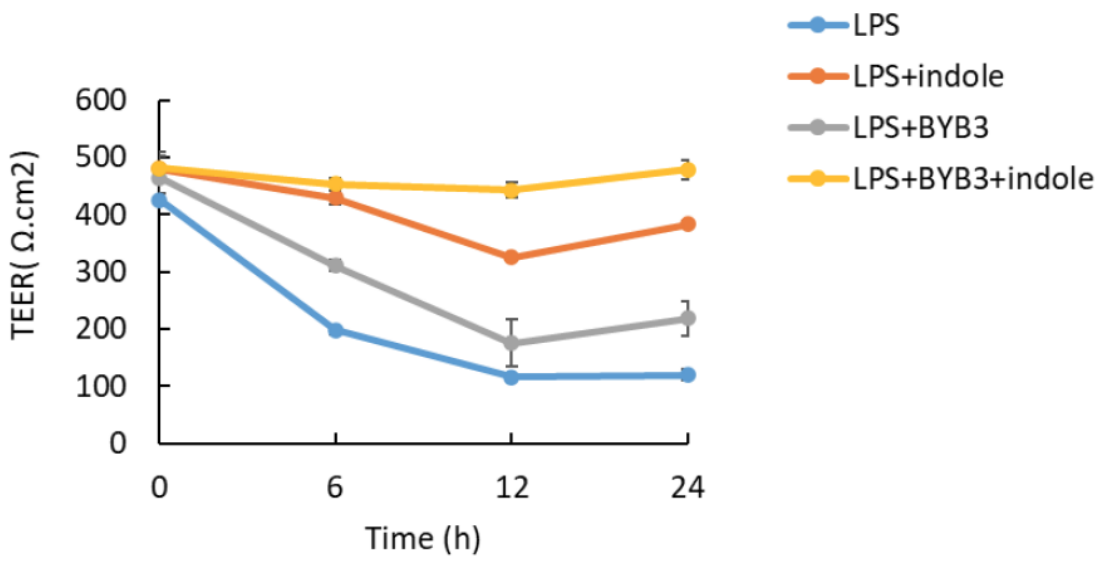

Fig. 3. Metabolites of *L. curvatus* BYB3 and indole increased the TEER in LPS-treated Caco-2 cells

Metabolites of *L. curvatus* BYB3 and indole significantly increased the TEER of Caco-2 cell monolayers in response to an inflammatory stimulus (LPS). After incubation with 10 ng/mL of LPS, the supernatants were incubated with indole, *L. curvatus* BYB3, and BYB3+indole from 0 to 24 h. The data are presented as the mean ± SD (n = 3). Statistically significant differences are shown by *p< 0.05 and **p< 0.01.

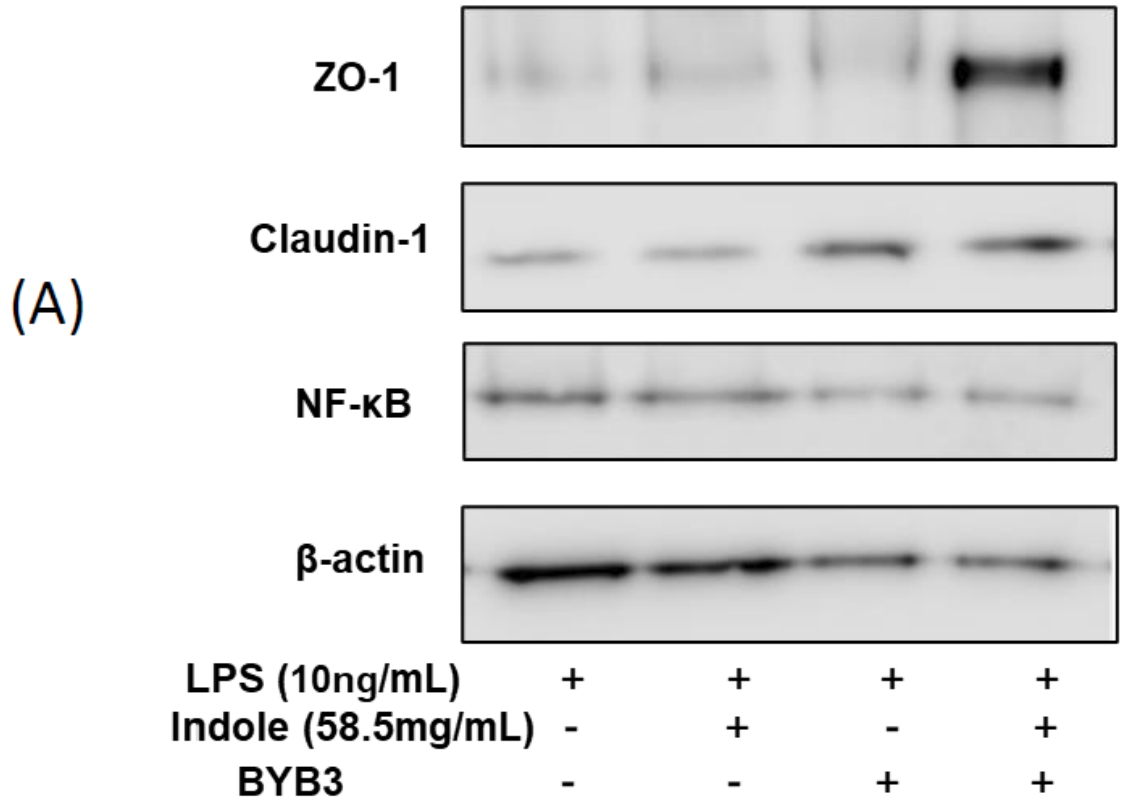
ZO-1
Claudin-1
NF-κB
β-actin
LPS (10ng/mL) + + + +
Indole (58.5mg/mL) - + - +
BYB3 - - + +

(A)

504

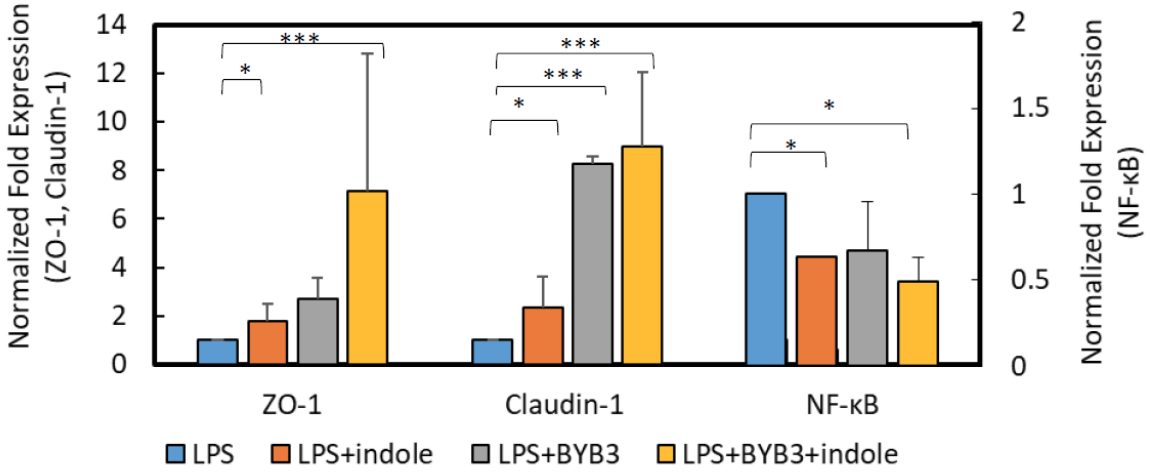
Normalized Fold Expression (ZO-1, Claudin-1)
Normalized Fold Expression (NF-κB)
0
2
4
6
8
10
12
14
0
0.5
1
1.5
2
*
***
ZO-1
Claudin-1
NF-κB
LPS
LPS+indole
LPS+BYB3
LPS+BYB3+indole

(B)

505

Fig. 4. Expression of TJ proteins and inflammatory responses

Caco-2 cells were co-treated with 10 ng/ mL of LPS and indole, *L. curvatus* BYB3, and BYB3+indole for 24 h. Cells treated with LPS (10 ng/mL) alone served as the control. LPS down-regulated the expression of ZO-1 and claudin-1, increased paracellular permeability, and disrupted the epithelial membrane integrity (A). Protein expression was restored in the treatment groups. The metabolites of the *L. curvatus* BYB3+indole group showed the most significant increase in ZO-1 expression and a decrease in NF-κB expression. Graph (B) showed the ratios of the proteins ZO-1, claudin-1, and NF-κB, respectively, according to the β-actin calculated from the band density via western blots analysis (*$p < 0.05$, **$p < 0.01$, ***$p < 0.001$ compared with the control, $n = 3$).

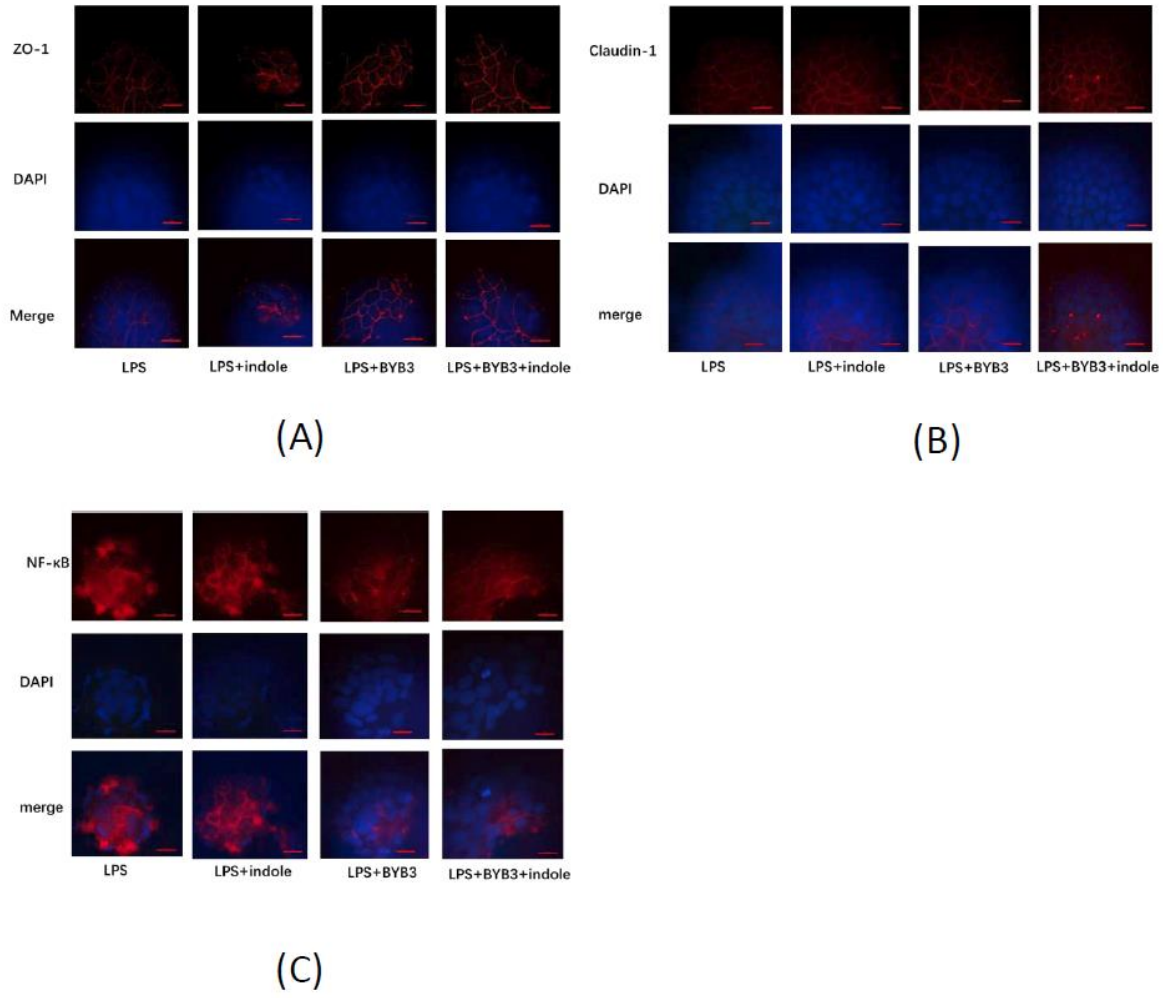

517

518 **Fig. 5. Immunofluorescence of the localization and expression of TJ proteins**

519 The supernatants of the indole and *L. curvatus* BYB3, and the metabolites of
520 BYB3+indole treatment groups modulated the expression of (A) ZO-1, (B) claudin-1, and (C)
521 NF-κB in differentiated Caco-2 cells exposed to an inflammatory stimulus. Caco-2 cells were
522 differentiated and treated with 10 ng/ mL of LPS (control) for 24 h. The control demonstrated
523 severe disruption of the tight junction proteins. Co-treatment with supernatants of LPS, indole,
524 and *L. curvatus* BYB3+indole improved the ZO-1 protein expression. However, the group
525 treated with LPS and the metabolites of *L. curvatus* BYB3+indole displayed more
526 improvement than those co-treated with LPS+indole and LPS+BYB3. (A) A similar trend was
527 observed for the expression of claudin-1. (B) The metabolites of *L. curvatus* BYB3+indole
528 suppressed the LPS-induced activation of NF-κB. (C) The reduction observed with the co-

529 treatment of LPS+indole and LPS+BYB3 was lower than that observed in the group co-treated
530 with LPS and metabolites of *L. curvatus* BYB3+indole (n = 3).

531

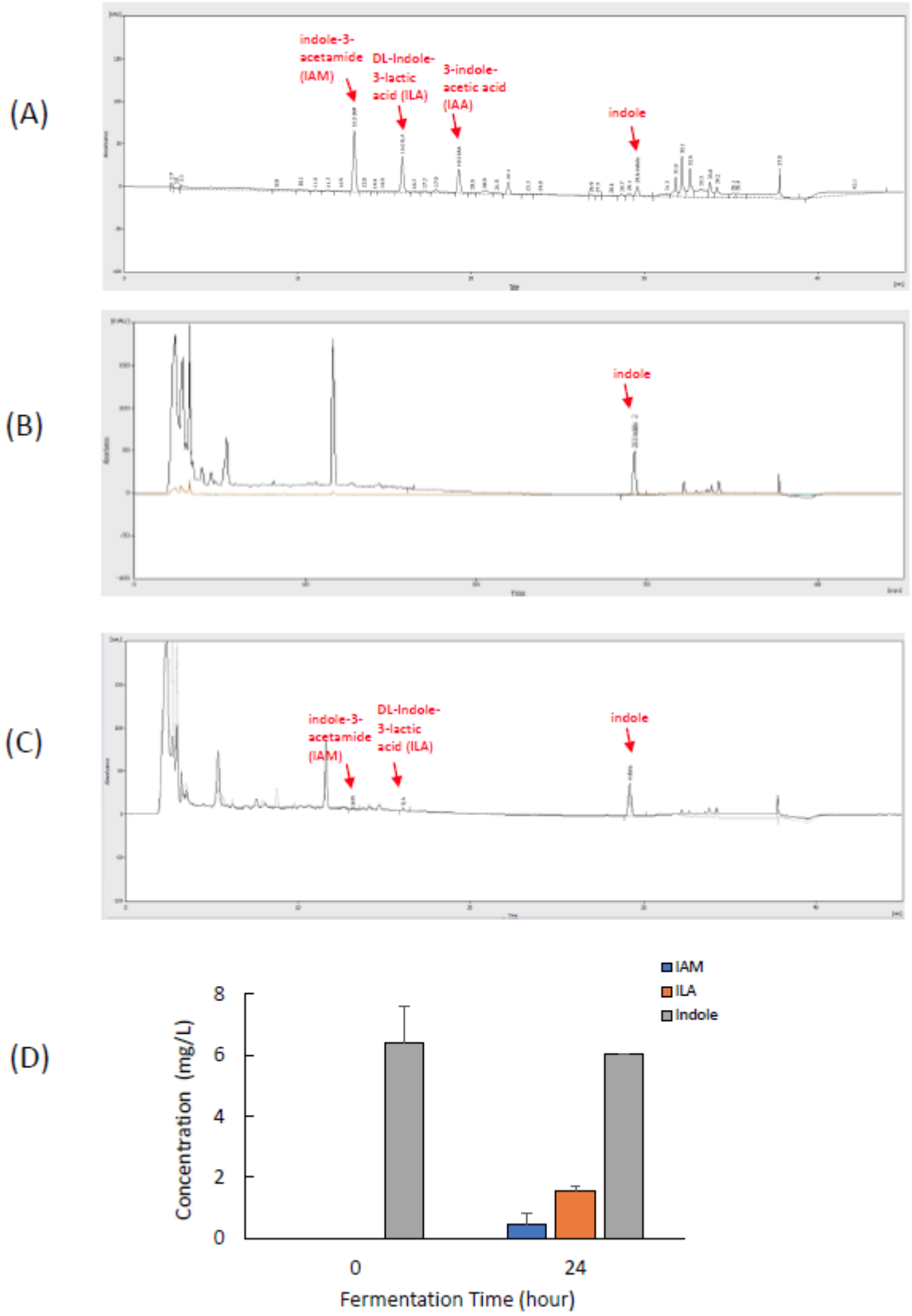

532

533 **Fig. 6. HPLC chromatographs of samples' indole compounds**

(A) Indole and indole derivates (ILA, IAA, and IAM) at 280 nm and UV spectra of 200–400 nm. (B, C) 0 and 24 h fermentation supernatants of *L. curvatus* BYB3+indole samples. (D) Indole and indole derivatives (ILA and IAM) in the supernatants of the 0 and 24 h fermentations of *L. curvatus* BYB3+indole samples (n = 3).